Vietnam Journal of Science and Technology ***63*** *(2) (2025) 378-387*
doi:10.15625/2525-2518/19491

A comparison of benzene-core PCF optical characteristics with hexagonal and circular lattices

Le Tran Bao Tran, Chu Van Lanh*

Department of Physics, Vinh University, 182 Le Duan, Vinh City, Nghe An Province, Viet Nam

*Email: *chuvanlanh@vinhuni.edu.vn*

Received: 25 November 2023; Accepted for publication: 6 March 2025

Abstract. This work compares the optical characteristics of benzene photonic crystal fiber with hexagonal lattice (H-PCF) and circular lattice (C-PCF). The difference in the radius between the rings is used to optimize effective area, nonlinearity, attenuation, and chromatic dispersion simultaneously. A series of numerical studies show that the effective mode area and attenuation are small for C-PCF and large for H-PCF geometries. That is the reason why the nonlinear coefficient of H-PCF is larger. Meanwhile, flat dispersion over a wide wavelength range is achieved mostly with H-PCFs in both dispersion modes. Our optimized fibers with near-zero flat dispersion, small loss, and large nonlinearity can enhance supercontinuum generation efficiency to generate a broad spectrum with high coherence.

Keywords: Photonic crystal fiber, nonlinearity, circular lattice, dispersion, hexagonal lattice.

Classification numbers: 4.2.2, 4.10.4.

1. INTRODUCTION

Photonic crystal fiber (PCF) with different light-guiding mechanisms has led to a wide range of applications in telecommunications, biomedicine, spectroscopy, sensing, etc. [1, 2]. First, total internal reflection is enabled in an index-guided PCF consisting of micrometer-sized air holes surrounding a solid core. The other is called a photonic band gap, in which light is guided in a hollow core with a low refractive index. Note that the unique properties of PCF come from the flexibility in the design model [3 - 5]. To apply it to a specific field, structural parameters such as hole pitch, air hole size, lattice shape even materials used can be adjusted until the desired purpose is achieved. That is the reason why its optical characteristics, such as chromatic dispersion, can be controlled as much as possible [6 - 8]. For supercontinuum generation (SG) application, the optical fiber should exhibit flat dispersion, high nonlinearity, and low attenuation. It is difficult to achieve these simultaneously in a PCF with equally sized air holes in the cladding since it only controls dispersion and not other features. A typical method to meet the criteria for dispersion and light transmission at the same time is a cladding containing different air holes. By this method, the dispersion curve is flattened and the attenuation in PCFs can be decreased [6].

Rectangular cladding with high birefringence and square one with high symmetry are proposed as alternatives to the hexagonal lattice PCFs (H-PCFs). However, the actual fabrication

of the former and the light confinement of the latter are not trivial problems [9, 10]. Recently, circular lattice PCFs (C-PCFs) have gradually attracted more attention [11 - 14]. These fibers are also excellent candidates for inline dispersion compensation in broadband applications.

This work aims to design structures of benzene-filled H-PCFs and C-PCFs with differences in the radius of the air holes for simultaneous optimization of effective area, nonlinear coefficient, attenuation, and chromatic dispersion in the 500 - 2000 nm wavelength range. To further increase the nonlinearity of the fiber, the core is filled with a highly nonlinear liquid such as benzene which has a nonlinear refractive index 61 times larger than that of silica (n_2 (benzene) = 1.68×10^{-18} m^2/W) [15]. The results obtained from the above two types of structures are then compared to find the most optimal structure for the SG. Although the study of these two lattices has been mentioned in a publication [16], the authors only investigated the dispersion characteristics of PCFs. Recently, we have conducted numerical simulations of the optical properties of benzene-core PCFs with individual lattices such as hexagonal [17], square [18], and circular lattices [19]. On this basis, the linear and nonlinear optical features of the fundamental modes for different lattice structures were compared in the all-normal dispersion regime [20]. Here, we consider the optical characteristics of benzene-filled H-PCFs and C-PCFs in the all-normal dispersion and anomalous dispersion cases with one and two zero-dispersion wavelengths (ZDWs) for SG with broad and flat spectra.

The structure of the paper is organized as follows: In section 2, we introduce the geometrical parameters of the benzene-core H-PCF and C-PCF along with some optical properties of the materials used. Section 3 presents the basic theories of light propagation and the simulation results of the optical properties of H-PCFs and C-PCFs. The optimum fibers are proposed based on the dispersion curves. Other optical features of the selected PCFs are also compared to highlight the advantages of each lattice type. Finally, the main results of the paper are concluded in section 4.

2. OPTICAL AND GEOMETRICAL PARAMETERS OF PCF

Designed fibers include three materials with the core's greatest refractive index and the air holes' smallest refractive index. Our PCFs consist of a benzene core, air holes, and silica substrate with refractive index n_1, n_2, and n_3, respectively, where r_c is the core radius (Figure 1).

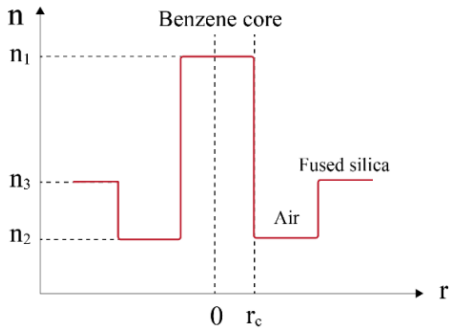

Figure 1. Refractive index profile of benzene PCFs.

The refractive index $n(\lambda)$ of benzene and fussed silica is calculated based on Cauchy and Sellmeier equations given by [15]:

$$n_{benzene}(\lambda) = \sqrt{B_0 + B_1\lambda^2 + B_2\lambda^{-2} + B_3\lambda^{-4} + B_4\lambda^{-6}} \quad (1)$$

$$n_{silica}(\lambda) = \sqrt{1 + \sum_{i=0}^{2}\left(S_i\lambda^2 / \lambda^2 - l_i^2\right)} \quad (2)$$

where B_0, B_1, B_2, B_3, B_4, S_i, and l_i are presented in Table 1.

We have considered the benzene-core structure of H-PCF as depicted in Figure 2a and compared it with the C-PCF (Figure 2b).

Table 1. The material coefficients.

Material	Coefficients					
	B_0	B_1 (μm^2)	B_2 (μm^2)	B_3 (μm^4)	B_4 (μm^6)	
Benzene	2.170184597	0.00059399	0.02303464	-0.000499485	0.000178796	
	S_0	l_0 (μm^2)	S_1	l_1 (μm^2)	S_2	l_2 (μm^2)
Fused silica	0.6694226	0.066933549	0.4345839	0.1152605744	0.8716947	9.7642963

Both types of lattices possess eight layers of air holes with a radius of r except for the first ring (r_1). We define the air-filling fraction as $f = 2r/\Lambda$. To maintain the behavior of a single-mode fiber over a spectrum and decline the impact of longitudinal inhomogeneities, the f-ratio must be less than a certain value. In this study, we use the filling factor of the first ring ($f_1 = 2r_1/\Lambda$) between 0.3 and 0.8 and the filling factor of the outer rings $f = 0.95$ for simultaneous optimization of the optical features of PCF [21]. The pitch length Λ is gradually extended from 1 μm to 2.5 μm (0.5 μm steps). The above geometric parameters lead to a small core ($r_c = \Lambda - 1.1r_1$) that ensures the fibers are all single-mode.

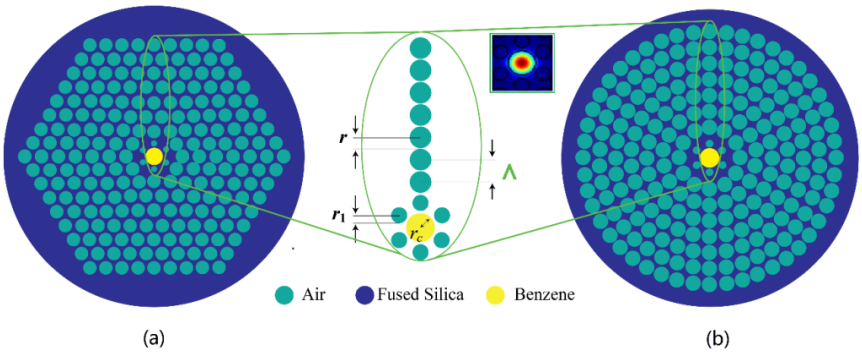

Figure 2. Cross-sections of H-PCFs (a) and C-PCFs (b) infiltrated with benzene.

3. METHODS AND SIMULATION RESULTS

Chromatic dispersion $D(\lambda)$ in [ps/nm/km], the cause of the broadening of optical pulses, is calculated concerning the real part of the effective refractive index Re[n_{eff}] [22]:

$$D(\lambda) = -\left(\lambda / c\right) \times \left(d^2\,\mathrm{Re}[n_{eff}] / d\lambda^2\right) \quad (3)$$

where c is the velocity of light in the vacuum. The effective refractive index n_{eff} is a value that quantifies the phase delay per unit length in a waveguide compared to the phase delay in a vacuum. It is defined by the relationship [23]:

$$n_{eff} = \beta / k = \beta\lambda / 2\pi \quad (4)$$

where β is the propagation constant of the guided mode (or the magnitude of the guided-mode wavevector along the fiber axis) and k represents the free-space wavevector [23].

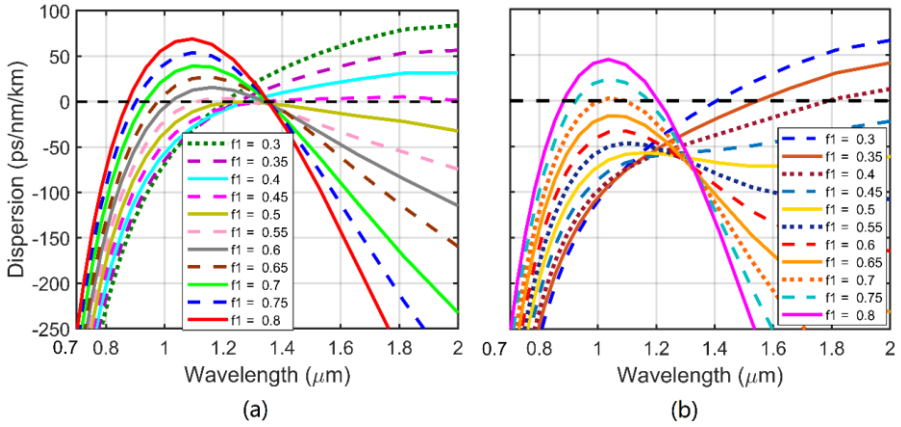

Figure 3. Dispersion curves of H-PCFs (a) and C-PCFs (b) for f_1 = 0.3-0.8 and Λ = 1 μm.

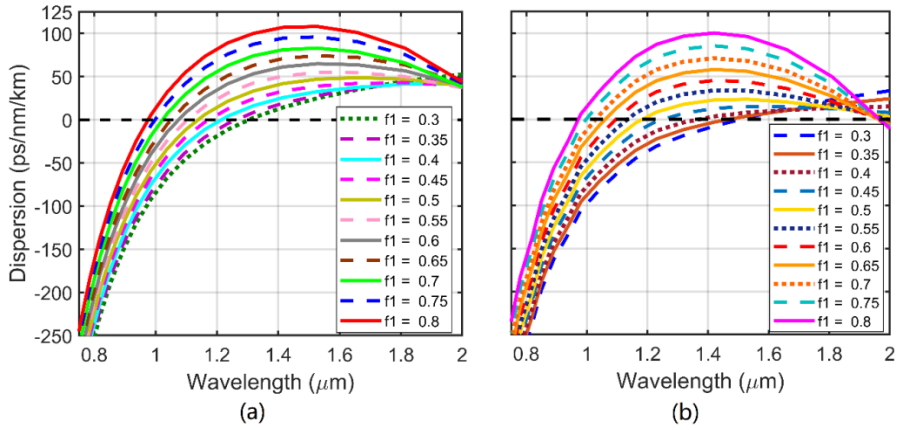

Figure 4. Dispersion curves of H-PCFs (a) and C-PCFs (b) for f_1 = 0.3-0.8 and Λ = 1.5 μm.

Numerical simulations of the optical properties of benzene-core H-PCFs and C-PCFs are performed using Lumerical MODE Solutions based on the full-vectorial finite-difference method [24]. From the obtained data, we plot the dispersion curves of all the structures with the help of Matlab software as shown in Figures 3-6. Figure 3 indicates the dispersion characteristics of benzene-filled H-PCFs and C-PCFs in the case of Λ = 1 μm. While H-PCFs possess only one all-normal dispersion curve, this regime appears commonly in C-PCFs. A similar behavior is observed for anomalous dispersion with one ZDW. This demonstrates that the dispersion curves with two ZDWs dominate in H-PCFs. The interaction between waveguide dispersion and material dispersion becomes stronger as Λ increases [25], making the dispersion curves noticeably flatter (Figures 4-6). At Λ = 1.5 μm, several dispersion curves with one ZDW (f_1 = 0.3 - 0.5) and two ZDWs (f_1 = 0.55 - 0.8) can be obtained in C-PCFs. In contrast, when Λ is larger than 1 μm, H-PCFs always maintain a dispersion regime with one ZDW over the entire wavelength range. In particular, ZDWs tend to shift toward the optical windows (e.g. 1.3 and

1.55 μm) according to the decrease of f_1, facilitating the selection of the pump wavelength in the smallest loss region.

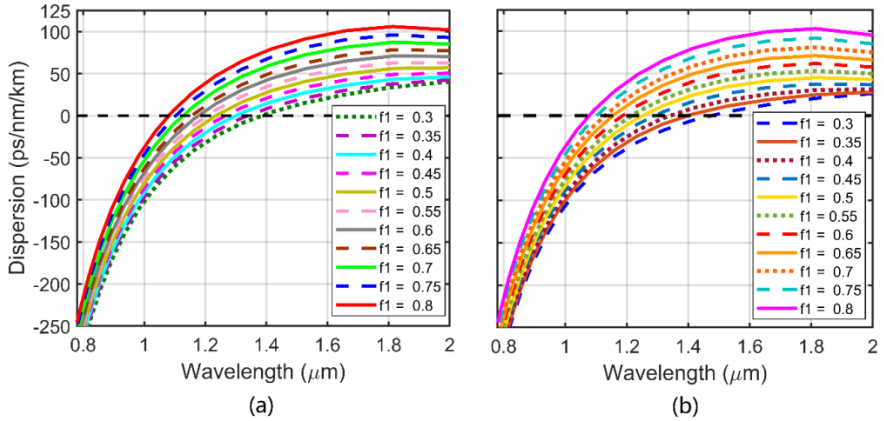

Figure 5. Dispersion curves of H-PCFs (a) and C-PCFs (b) for f_1 = 0.3-0.8 and Λ = 2 μm.

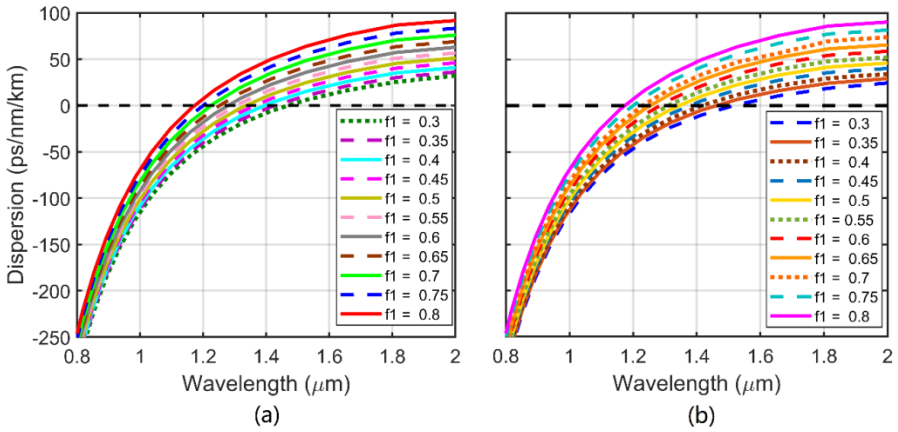

Figure 6. Dispersion curves of H-PCFs (a) and C-PCFs (b) for f_1 = 0.3 - 0.8 and Λ = 2.5 μm.

The smooth and highly coherent supercontinuum spectrum requires a fiber with flat all-normal dispersion in the wavelength range of investigation. The dispersion curve is considered flat when its slope is small with an absolute value of dispersion ≤ 10 ps/nm/km, preferably equal to or less than 5 ps/nm/km (called ultra-flat dispersion) [26, 27]. On that basis, two fiber designs are selected with the following structural parameters: H-PCF$_1$ with Λ = 1 μm, f_1 = 0.5 and C-PCF$_1$ with Λ = 1 μm, f_1 = 0.65 (Figure 7a). It can be observed that H-PCF$_1$ has near-zero flattened dispersion in the wavelength range of 1.11 - 1.53 μm with a bandwidth of 420 nm. This range is broader than the flat dispersion region of C-PCF$_1$ and some previous publications on liquid-core PCFs with uniform and non-uniform air holes [16, 28, 29]. The expected pump wavelengths are 1.3 μm for H-PCF$_1$ and 1.064 μm for C-PCF$_1$.

We choose fiber pairs with near-zero flat dispersion in the anomalous dispersion regime to achieve a broad SG in the near-infrared range. These are H-PCF$_2$ with Λ = 2.5 μm, f_1 = 0.3 and C-PCF$_2$ with Λ = 2 μm, f_1 = 0.3 (one ZDW, Figure 7b), and H-PCF$_3$ with Λ = 1 μm, f_1 = 0.55 and C-PCF$_3$ with Λ = 1 μm, f_1 = 0.7 (two ZDWs, Figure 7c). It can be seen that C-PCF$_2$ fiber which

has ZDW at 1.48 μm is not much different from H-PCF$_2$ in terms of closeness to zero dispersion. The pump laser is used for two structures with the same wavelength of 1.5 μm.

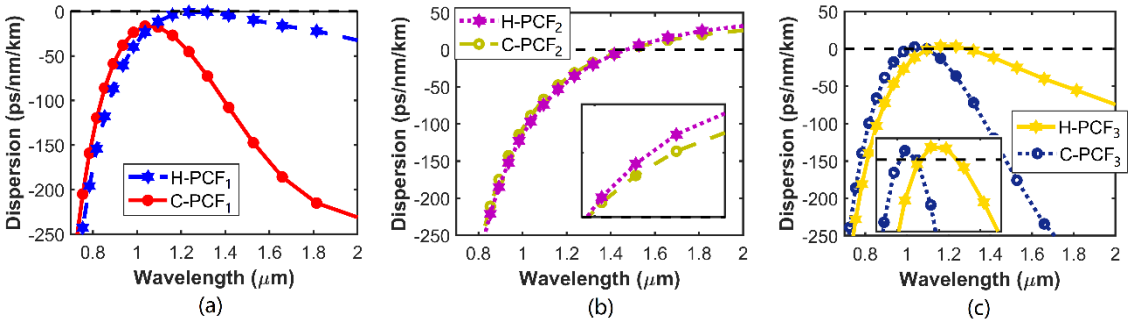

Figure 7. Dispersion curves of the proposed H-PCFs and C-PCFs with (a) all-normal dispersion, (b) one ZDW, and (c) two ZDWs.

In the remaining case, the hexagonal lattice again shows an advantage in dispersion characteristics. This means that H-PCF$_3$ has a flat dispersion curve over a wider wavelength range than C-PCF$_3$, although the deviation from zero dispersion between the two fibers is negligible. The ZDWs are 1.11 and 1.28 μm for H-PCF$_3$, 1.01 and 1.09 μm for C-PCF$_3$. Therefore, H-PCF$_3$ is pumped at 1.2 μm while C-PCF$_3$ has 1.064 μm of pump wavelength.

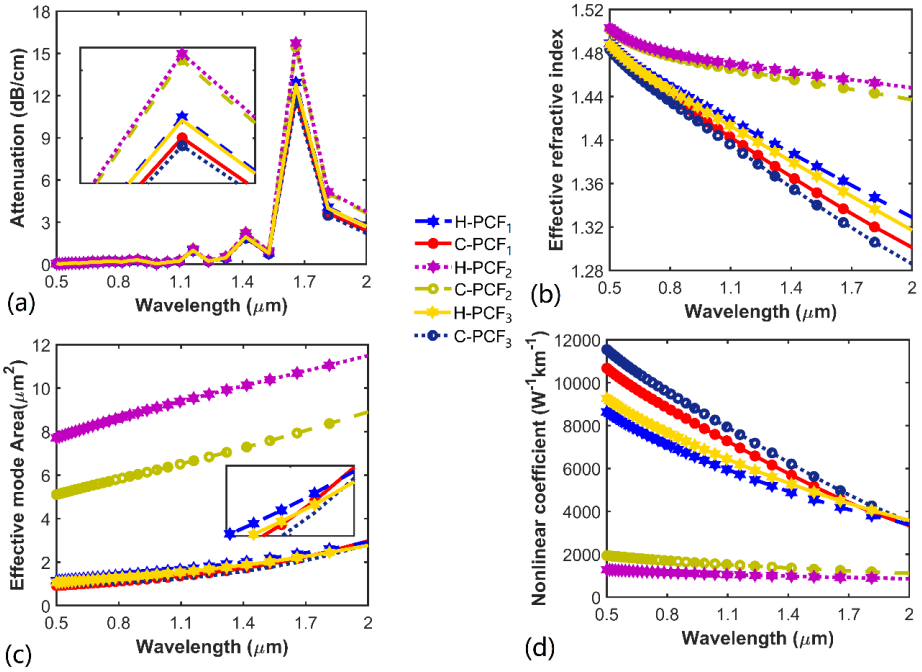

Figure 8. Optical characteristics of the proposed H-PCFs and C-PCFs: (a) attenuation, (b) effective refractive index, (c) effective mode area, and (d) nonlinear factor.

After proposing optimum PCFs corresponding to each distinct dispersion regime, we continue to synthesize other optical characteristics of these fibers including attenuation, effective refractive index, effective mode area, and nonlinear factor in the graphs of Figure 8. Figure 8a illustrates the modification in the attenuation for the proposed fibers. The attenuation is

approximately zero from 0.5 μm to 1.1 μm. It then increases gradually until reaching a peak at 1.66 μm before dropping in the next wavelength region. This similar trend of six structures is determined mainly by material loss without the influence of confinement loss [29]. H-PCF_2 and C-PCF_2 have the greatest attenuation among the proposed fibers, followed by the remaining H-PCFs and C-PCFs. These two fibers also have low nonlinear coefficients originating from their large effective refractive index and large effective mode area [19]. Low-loss structures, e.g. C-PCF_1 and C-PCF_3 have small effective mode areas resulting in their high nonlinearity. This can be explained by the expression [23]:

$$\gamma(\lambda) = 2\pi n_2 / \lambda A_{eff} \quad (5)$$

where γ denotes the nonlinear coefficient and A_{eff} is the effective mode area.

Table 2. The values of optical characteristics of the proposed structures.

Proposed PCFs	Optical characteristics					
	Dispersion (ps/nm/km)	Attenuation (dB/cm)	Effective refractive index	Effective mode area (μm^2)	Nonlinear factor (W^{-1} km^{-1})	Pump wavelength (μm)
H-PCF_1	-0.89	0.42	1.398	1.9	5255.9	1.3
C-PCF_1	-16.99	0.19	1.407	1.3	7447.8	1.064
H-PCF_2	3.2	1.27	1.46	10.3	960	1.5
C-PCF_2	2.1	1.25	1.453	7.4	1320.3	1.5
H-PCF_3	3.3	0.59	1.402	1.6	6046.1	1.2
C-PCF_3	1.3	0.19	1.4	1.2	8107.1	1.064

The optical characteristics of the optimized fibers calculated at the pump wavelength are presented in Table 2. This table and Figure 7 show that the H-PCF has the advantage of small and flat dispersion, whereas C-PCFs obtain a smaller effective mode area and low loss due to their high symmetry (Figure 8). The nonlinear coefficients of the two types of structures are exceptionally high, especially for PCFs with all-normal dispersion and anomalous dispersion with two ZDWs. For example, the nonlinearity profiles of H-PCF_3 and C-PCF_3 are 6046.1 W^{-1} km^{-1} and 8107.1 W^{-1} km^{-1}, respectively. These values are 32 and 43 times higher than the nonlinear coefficients of the publication [28]. On the other hand, our structures have quite small losses compared to previous liquid core PCFs [11, 30]. The above excellent properties are achieved thanks to the structure with differences in air-hole radius between the rings.

4. CONCLUSIONS

This work concentrates on optimizing optical features in benzene-core H-PCFs and C-PCFs with the various radii of air-hole rings. The simulation results show that the small effective mode area is obtained for C-PCF designs and the large one appears in H-PCFs. The attenuation of C-PCFs is especially lower than that of H-PCFs. Flat dispersion over a wide wavelength range is achieved mostly with H-PCFs although its value at the pump wavelength is not significantly different from that of C-PCFs. Our optimized fibers with near-zero flat dispersion, small loss, and large nonlinearity can enhance SG efficiency to generate a broad spectrum with high coherence.

The PCFs proposed in this work are being experimentally investigated for real fiber production in our ongoing project. The fabrication process of a fiber following the stack-and-draw method includes several basic steps [31]: First, large silica tubes/rods are drawn into small

tubes 1 m long with an outer diameter of a few millimeters. These tubes have the same air-filling ratio as the cladding region. The next step is to stack the fused silica capillaries according to the proposed PCF pattern. The stack is then inserted into a circular glass tube to form an outer protective layer. After being fixed on the top of the fiber drawing tower, the preform is put into a high-temperature furnace at about 2000°C to draw into thinner fibers with guaranteed structural parameters as the original sample. A selective liquid infiltration process is considered to fill the core with benzene [32]. After the real fibers are fabricated, their dispersion properties are measured by a white-light spectral interferometric technique in a standard Mach-Zehnder interferometer setup [33]. On the other hand, the attenuation of the tested fibers is measured by the cut-back method [34]. The experimental data are then compared with numerical simulation results using real fiber geometrical parameters.

Acknowledgements. This research is supported by Vietnam National Foundation for Science and Technology Development (NAFOSTED) under grant number 103.03-2023.01, and the Master, PhD Scholarship Programme of Vingroup Innovation Foundation (VINIF), code VINIF.2023.TS.133.

CRediT authorship contribution statement. Le Tran Bao Tran: Investigation, Formal analysis, Visualization, Data curation, Writing – original draft. Chu Van Lanh: Conceptualization, Methodology, Supervision, Writing – original draft, Writing – review & editing.

Declaration of competing interest. The authors declare that they have no known competing financial interests or personal relationships that could have appeared to influence the work reported in this paper.

REFERENCES

1. Xue P., Liu Q., Lu S., Xia Y., Wu Q., Fu Y. - A review of microstructured optical fibers for sensing applications, Optical Fiber Technol. **77** (2023) 103277. doi.org/10.1016/j.yofte.2023.103277
2. Ahmed K., Islam M. I., Paul B. K., Islam M. S., Sen S., Chowdhury S., Uddin M. S., Asaduzzaman S., Bahar A. N. - Effect of photonic crystal fiber background materials in sensing and communication applications, Mat. Discovery **7** (2017) 8-14. doi.org/10.1016/j.md.2017.05.002
3. Agrawal G. P. - Applications of Nonlinear Fiber Optics. Academic Press, New York, 2021.
4. Bunge C., Gries T., Beckers M. - Polymer Optical Fibres, Woodhead Publishing, Sawston (2017)
5. Kumar P., Kumar V., Roy J. S. - Design of quad core photonic crystal fibers with flattened zero dispersion, AEU – Int. J. Electron. Communications **98** (2019) 265-272. doi.org/10.1016/j.aeue.2018.11.014
6. Tran L. T. B., Minh N. H., Dung T. T., Anh T. D., Duy L. P., Phuong N. T. H., Luu M. V., Thuy D. T., Lanh C. V. - Numerical study of linear optical properties of As_2S_3 glass PCF taking into account the difference in structural parameters, Adv. Opt. Photon. Spectros. Appl. XII (2022) 305-312.
7. Pan C., Han Y., Lu J. - Design and Optimization of Lattice Structures: A Review, Appl. Sci. **10** (18) (2020), 6374. doi.org/10.3390/app10186374
8. McClung A., Mansouree M., Arbabi A. - At-will chromatic dispersion by prescribing light trajectories with cascaded metasurfaces, Light Sci. Appl. **9** (2020) 93. doi.org/10.1038/s41377-020-0335-7

9. Kim S., Kee C., Lee G. L. - Modified rectangular lattice photonic crystal fibers with high birefringence and negative dispersion, Opt. Express **17** (10) (2009) 7952-7957. doi.org/10.1364/OE.17.007952
10. Hossain S., Shah S., Faisal M. - Ultra-high birefringent, highly nonlinear $Ge_{20}Sb_{15}Se_{65}$ chalcogenide glass photonic crystal fiber with zero dispersion wavelength for mid-infrared applications, Optik **225** (2021) 165753. doi.org/10.1016/j.ijleo.2020.165753
11. Trong D. V., Lanh C. V. - Broadband Supercontinuum Generation with Low Peak Power in a Circular Lattice Nitrobenzene-Core Photonic Crystal Fiber, Bull. Lebedev Phys. Inst. **50** (2023) 318-331. doi.org/10.3103/S1068335623080080
12. Shahriar T. A. M. R., Islam O., Tahmid M. I., Alam M. Z., Alam M. S. - Highly coherent supercontinuum generation in circular lattice photonic crystal fibers using low-power pulses, Optik **272** (2023) 170258. doi.org/10.1016/j.ijleo.2022.170258
13. Khalek M. A., Chakma S., Ahmed K., Paul B. K., Vigneswaran D., Zakaria R. - Materials Effect in Sensing Performance Based on Surface Plasmon Resonance Using Photonic Crystal Fiber, Plasmonics, **14** (2019) 861-867. doi.org/10.1007/s11468-018-0867-3
14. Rjeb A., Fathallah H., Chebaane S., Machhout M. - Design of novel circular lattice photonic crystal fiber suitable for transporting 48 OAM modes, Optoelectron. Lett. **17** (8) (2021) 501-506. doi.org/10.1007/s11801-021-0158-7
15. Duc H. T., Tu N. A., Thuy N. T. - A New Design of Ultra-flat Dispersion Photonic Crystal Fiber using Benzene Infiltration, VNU J. Sci. Mathematics - Physi. **39** (1) (2023) 42-52. doi.org/10.25073/2588-1124/vnumap.4762
16. Tran L. T. B., Oanh T. T. C., Thuy N. T., Lanh C. V. - Comparison of chromatic dispersion of circular and hexagonal photonic crystal fibers with chloroform-core, Majlesi J. Electrical Engineering **16** (3) (2022) 55-61. doi.org/10.52547/mjee.16.3.55
17. Tran L. T. B., Lanh C. V. - A new type of supercontinuum generation in hexagonal lattice C_6H_6-core PCF with broadband and low-power pump, Int. J. Mod. Phys. B **38** (26) (2024) 2450353. doi.org/10.1142/S0217979224503533
18. Tran L. T. B., Lanh C. V. - Simultaneous optimization of optical characteristics of square-shaped benzene-core photonic crystal fiber based on non-uniform air holes, Majlesi J. Electrical Engineer. **18** (1) (2024) 241-251. doi.org/10.30486/mjee.2024.2000133.1307
19. Tran L. T. B., Lanh C. V. - Circular lattice benzene-core PCFs with flat near-zero dispersion for the low-power broad-spectrum supercontinuum generation, Phys. Scr. **99** (4) (2024) 045527. doi.org/10.1088/1402-4896/ad347c
20. Lanh C. V., Tran L. T. B., Thuy N. T., Duc H. T., Trong D. V., Trang D. M., Hoang T. N., Thanh T. D., Khoa D. Q. - Comparison of supercontinuum generation spectral intensity in benzene-core PCFs with different types of lattices in the claddings, Opt. Quant. Electron. **54** (12) (2022) 840. doi.org/10.1007/s11082-022-04218-1
21. Saitoh K., Koshiba M., Hasegawa T., Sasaoka E. - Chromatic dispersion control in photonic crystal fibers: application to ultra-flattened dispersion, Opt. Express **11** (8) (2003) 843-852. doi.org/10.1364/OE.11.000843
22. Lanh C. V, Anuszkiewicz A., Ramaniuk A., Kasztelanic R., Khoa D. X., Van C. L, Trippenbach M., Buczyński R. - Supercontinuum generation in photonic crystal fibres with core filled with toluene, J. Opt. **19** (2017) 125604. doi.org/10.1088/2040-8986/aa96bc

23. Dudley J. M., Taylor J. R., - Supercontinuum Generation in Optical Fibers, Cambridge University Press, United Kingdom, 2010.
24. Obayya S., Hameed M. F. O., Areed N. F. F. - Computational Liquid Crystal Photonics: Fundamentals, Modelling and Applications, John Wiley & Sons, Ltd., United Kingdom, 2016.
25. Lee Y. S., Lee C. G., Bahloul F., Kim S., Oh K. - Simultaneously Achieving a Large Negative Dispersion and a High Birefringence Over Er and Tm Dual Gain Bands in a Square Lattice Photonic Crystal Fiber, J. Lightwave Technol. **37** (4) (2019) 1254-1263. doi.org/10.1109/JLT.2019.2891756
26. Hirano M., Tetsuya N., Okuno T. - European patent application published in accordance with Art. **158** (3) EPC, European Patent Office, Patent Application No. EP2008XXXX, 2008.
27. Grzesiak M., Poturaj K., Makara M., Mergo P. - Optical fiber with varied flat chromatic dispersion, Opt. Fiber Technol. **88** (2024) 103972. doi.org/10.1016/j.yofte.2024.103972
28. Hieu L. V., Thuy H. V., Hue N. T., Van C. L., Buczyński R., Kasztelanic R. - Supercontinuum generation in photonic crystal fibers infiltrated with tetrachloroethylene, Opt. Quant. Electron. **53** (2021) 187. doi.org/10.1007/s11082-021-02820-3
29. Thuy N. T., Duc H. T., Tran L. T. B., Trong D. V., Lanh C. V. - Optimization of optical properties of toluene-core photonic crystal fibers with circle lattice for supercontinuum generation, J. Opt., **51** (3) (2022) 678-688. doi.org/10.1007/s12596-021-00802-y.
30. Trong D. V., Lanh C. V. - Supercontinuum generation in $C_6H_5NO_2$-core photonic crystal fibers with various air-hole size, Mod. Phys. Lett. B **37** (22) (2023) 2350063. 10.1142/S021798492350063X
31. Murphy L. R., Yerolatsitis S., Birks T. A., Stone J. M. - Stack, seal, evacuate, draw: a method for drawing hollow-core fiber stacks under positive and negative pressure, Opt. Express **30** (21) (2022) 37303-37313. doi.org/10.1364/OE.470599
32. Thuy H. V., Kasztelanic R., Filipkowski A., Stępniewski G., Pysz D., Klimczak M., Ertman S., Van C. L., Woliński T. R., Trippenbach M., Khoa D. X., Śmietana M., Buczyński R. - Supercontinuum generation in an all-normal dispersion large core photonic crystal fiber infiltrated with carbon tetrachloride, Opt. Mat. Express **9** (5) (2019) 2264-2278. doi.org/10.1364/OME.9.002264
33. Thuy H. V., Kasztelanic R., Anuszkiewicz A., Stepniewski G., Filipkowski A., Ertman S., Pysz D., Wolinski T., Khoa D. X., Klimczak M., Buczyński R. - All-normal dispersion supercontinuum generation in photonic crystal fibers with large hollow cores infiltrated with toluene, Opt. Mat. Express **8** (11) (2018) 3568-3582. doi.org/10.1364/OME.8.003568
34. Hieu L. V., Thuy H. V., Stępniewski G., Trung L. C., Ngoc V. T. M., Kasztelanic R., Klimczak M., Pniewski J., Khoa D. X., Heidt A. M., Buczyński R. - Low pump power coherent supercontinuum generation in heavy metal oxide solid-core photonic crystal fibers infiltrated with carbon tetrachloride covering 930–2500 nm, Opt. Express **29** (24) (2021) 39586-39600. doi.org/10.1364/OE.443666